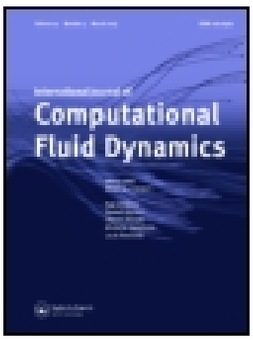

International Journal of Computational Fluid Dynamics

ISSN: 1061-8562 (Print) 1029-0257 (Online) Journal homepage: http://www.tandfonline.com/loi/gcfd20

A PRESSURE-BASED EULER SCHEME FOR TRANSONIC INTERNAL AND EXTERNAL FLOW SIMULATION

G. ZHOU & L. DAVIDSON

To cite this article: G. ZHOU & L. DAVIDSON (1995) A PRESSURE-BASED EULER SCHEME FOR TRANSONIC INTERNAL AND EXTERNAL FLOW SIMULATION, International Journal of Computational Fluid Dynamics, 5:3-4, 169-188, DOI: 10.1080/10618569508940741

To link to this article: http://dx.doi.org/10.1080/10618569508940741

Comp. Fluid Dyn., 1995, Vol. 5, p. 169–188
Reprints available directly from the publisher
Photocopying permitted by license only

A PRESSURE-BASED EULER SCHEME FOR TRANSONIC INTERNAL AND EXTERNAL FLOW SIMULATION

G. ZHOU and L. DAVIDSON

Department of Thermo and Fluid Dynamics, Chalmers University of Technology, S-412 96 Gothenburg, Sweden

(Received 25 August 1994; in final form 10 October 1994)

SUMMARY

The development of a pressure-based Euler scheme, based on a collocated grid arrangement and solving for Cartesian mass flux components is described. An implicit numerical dissipation model, which includes second and fourth difference terms expressed in pressure, is demonstrated. A smoothing function, which includes a two-level filter, is used to adjust the second order-dissipation. The successful calculations for the inviscid transonic aerodynamic flow around airfoil NACA0012 are presented. The transonic quasi-one-dimensional flow calculation in a converging-diverging nozzle is chosen as an example of an internal flow simulation.

KEY WORDS: Pressure-based method, collocated grids, numerical dissipation modeling, transonic flows, inviscid internal/external flows.

1. INTRODUCTION

A wide variety of solution schemes for the Euler equations have been developed during the last two decades. The extensive numerical experiments have shown that whether or not a scheme is efficient depends largely on the type of flow.

For transonic flow, density based methods (or time-marching schemes), for example the methods developed by Jameson[1], Rizzi[2] and Pulliam[3] have proved to be successful and powerful, especially for transonic aerodynamic flow simulations. However, for flows with very low Mach numbers, this type of method has to use artificial compressibility[4] to avoid the stiff problem, since density is nearly constant in these regions.

For incompressible flow, pressure-based methods, for example SIMPLE[5], SIMPLER[5] and PISO[6] have been widely used for many industrial applications. However, a problem, the poor shock capturing properties, arises when the methods are extended to compute transonic flows with shock discontinuities[7,8]. Even though the pressure-based method has been advanced and improved in many aspects recently, there are still few reports for inviscid transonic aerodynamic flow simulations in the literature. This paper presents the performance of a pressure-based Euler algorithm for transonic flows with good shock capturing properties.

For any type of scheme, proper artificial dissipation has to be introduced into the discretized transport equations, because the Euler equations do not provide natural dissipation mechanism that eliminates high frequencies caused by nonlinearities: For the density based methods, an artificial dissipation model which includes the second and fourth difference of the dependent variable, is widely used. However, for pressure-based methods, the task of finding a mechanism for introducing just enough artificial dissipation to damp the destabilizing effect arising from the elliptic nature of the pressure correction equation, while without smearing the physical discontinuity at shocks, is still a challenging task.

In earlier efforts[7-10] where pressure-based methods were applied to transonic flows, the velocity components (U, V) were used as the primary variables rather than, as in density based methods, the mass flux components $(\rho U, \rho V)$. Since the former variables vary much more rapidly across shocks than the latter, more numerical errors are included in solution. This results in heavy smearing in shock regions. Solving for the mass flux components is expected to reduce the discretization errors in the shock regions. McGuirk and Page[11], and more recently Lien and Leschziner[12], have shown that using mass flux components as the primary variables for the continuity and momentum equations, together with the retarded pressure or retarded density[13], is a wise choice. The mass flux component option allows for a direct relationship between momentum and pressure. The use of the retarded density concept with a certain filter makes it possible to introduce enough artificial dissipation so that both satisfactory stability and accuracy can be achieved.

In this paper, details of a recently developed calculation procedure are presented. The method is based on a finite volume code CALC-BFC[14], originally developed to solve the incompressible Navier-Stokes equation in a collocated grid arrangement, with Cartesian velocity components. The new algorithm uses the mass flux components as the transported variables. An implicit artificial dissipation model, which consists of a second-order and fourth-order differencing term of pressure, is used in all equations. This model is a combination of Rhie-Chow[9] type interpolation for mass flux and the retarded density concept. Different types of boundary conditions are adopted in the proposed scheme, depending on whether the flow is internal or external.

For external inviscid transonic airfoil flows, to our knowledge, few computations have been made using pressure-based methods. In this paper, successful computations of the internal quasi-one-dimensional flow in a converging and diverging nozzle, and the external flow around the NACA0012 airfoil are presented.

2. COMPUTATIONAL ALGORITHM

The Euler equations in integral form for an arbitrary stationary control volume δv with boundary $\delta\Omega$, and outer normal unit vector $\mathbf{n}$ at surface element ds, in a Cartesian reference frame, can be written as

$$\int_{\delta v} \frac{\partial \Phi}{\partial t} dv + \int_{\delta\Omega} \mathbf{F}\cdot\mathbf{n} ds = \int_{\delta v} S_\phi dv \tag{1}$$

where

$$\Phi = \begin{bmatrix} \rho \\ \rho \mathbf{V} \\ E \end{bmatrix}, \quad \mathbf{F} = \begin{bmatrix} \rho \mathbf{V} \\ \mathbf{V}\Phi \\ H\mathbf{V} \end{bmatrix}, \quad S_\phi = \begin{bmatrix} 0 \\ -\nabla P \\ 0 \end{bmatrix}$$

Here Φ is the vector of the conserved dependent variables, $\mathbf{F}$ is the flux tensor, S_ϕ is the source term, ρ, P are the fluid density and pressure, $\mathbf{V} = [U, V]^T$ where U, and V are the velocity components in the x and y directions, respectively. The Eq. (1) must be solved in conjunction with the perfect gas relationships,

$$H = C_P T + 0.5|\mathbf{V}|^2$$

$$P = \rho R T$$

In the two-dimensional steady adiabatic flow with enthalpy H = constant at infinity for external flows and at the inlet for internal flows, the correct steady-state solution can be obtained without solving the energy equation. So it is acceptable, as is done in the present work, to replace the energy equation by the assumption of constant enthaply $H = H_0$. In the present scheme the continuity equation is transformed into a pressure correction equation by using the truncated momentum equations. After the pressure correction is obtained, the pressure and mass flux component Φ are updated using the pressure correction. Then the density ρ can be related to pressure by the equation

$$\rho = \frac{\gamma P}{(\gamma - 1)(H_0 - 0.5|\mathbf{V}|^2)}. \tag{2}$$

2.1 *Spatial Discretization*

The physical domain is divided into quadrilateral control volumes. Since we use collocated stationary grids, all the geometrical properties of the transformation from physical domain to computational domain are calculated and stored.

To assure that a steady state solution independent of the time step, a semidiscrete approach which separates the space and time discretization can be used, where the spatial derivatives are approximated first.

All properties in the control volume are assumed to be averages. The volume integrals in Eq. (1) are expressed as

$$\int_{\delta v} \frac{\partial \Phi}{\partial t} dv = \frac{\partial \Phi}{\partial t} \int_{\delta v} dv = \frac{\partial \Phi}{\partial t} \delta \mathrm{v},$$

$$\int_{\delta v} S_\phi dv = S_\phi \int_{\delta v} dv = S_\phi \delta v.$$

The surface integral Eq. (1) over the boundary $\delta\Omega$ of the control volume is approximated by assuming the mean-value of the flux tensor on each side.

$$\int_{\delta\Omega} \mathbf{F}\cdot\mathbf{n}\,ds = \sum_{m=1}^{4} (\mathbf{F}\cdot\mathbf{A}) = \sum_{m=1}^{4} \{(\mathbf{V}\Phi)\cdot\mathbf{A}\} \tag{3}$$

where m refers to each face of the quadrilateral control volume. The flux $\mathbf{F}$ includes the convecting velocity $\mathbf{V}$ and the dependent variables Φ. All variables are located in the center of the cell (the control volume), while the flux $(\mathbf{F}\cdot\mathbf{A})$ has to be expressed at cell face m. So one needs some discretization approximations to get the cell-face values from the neighbouring cell-center values of Φ. In the implicit solution algorithm, the dependent variables Φ and the convecting velocity $\mathbf{V}$ could be expressed using different schemes.

For the value of dependent variables Φ in Eq. (3) at each cell faces, either the first-order upwind[5], second-order upwind[15], MUSCL[16], or third-order QUICK[17] and CHARM[18] schemes can be used.

For the convecting velocity $\mathbf{V}$, there is less choice than for Φ because of difficulties of discretization. A most convenient scheme is direct interpolation from cell-center values of Φ. However, oscillation in the solutions would be observed. It is attributable to the decoupling between velocity and pressure. To avoid this problem, one has to use either staggered grids[5-7] or a proper artificial viscosity model. This work uses an implicit artificial dissipation model which consists of second and fourth-order differences of pressure in all equations described later. The fourth-order terms of the numerical dissipation model are due to the use of Rhie-Chow interpolation[9], and the second-order terms are due to the use of retarded density[12,13], which is equivalent to the retarded pressure concept[11].

Since our interest is only in steady state without concern for time accuracy, we simply use a backward Euler implicit scheme for the time differencing. It is well known that a varying time step[19]

$$\Delta t \le \min\left[\frac{\Delta x}{c+|U|}, \frac{\Delta y}{c+|V|}\right] \tag{4}$$

(c denotes speed of sound) which corresponds to a uniform CFL number for the whole flow field can be used to enhance stability and the convergence rate for explicit schemes. The physical significance of this approach is that the varying time step Δt must be adjusted to less than or at most equal to the time required for a sound wave to propagate between two adjacent grid points. The use of the varying time step is also viewed as a way of the under-relaxation for the iterative scheme. Since the time dependent terms in this present algorithm are treated in an *implicit* fashion, practical time steps are set to

$$\Delta t = K[\min(\Delta t_\xi, \Delta t_\eta)]$$

where

$$\Delta t_\xi = \frac{\Delta\xi}{|\mathbf{V}\cdot\hat{\xi}|}, \quad \Delta t_\eta = \frac{\Delta\eta}{|\mathbf{V}\cdot\hat{\eta}|}$$

where the constant K could be larger than unity. ξ and η are the curvilinear coordinates $\hat{\xi}$ and $\hat{\eta}$ are unit vectors along the curvilinear coordinates.

All the discretizations described above are introduced into Eq (1), and we get the discretized equation as

$$(\Phi - \Phi^0)\frac{\delta v}{\Delta t} + \sum(\mathbf{F}\cdot\mathbf{A}) = S_\phi \delta v \tag{5}$$

where Φ^0 is the value at previous time level.

The final discretized equation can be cast into standard form

$$a_P \Phi_P = \sum a_{nb}\Phi_{nb} + S_C^\phi \tag{6}$$

where subscript nb denotes neighbour and

$$a_P = \sum a_{nb} - S_P^\phi.$$

The coefficients a_{nb} contain contributions from convection. S_C^ϕ contains the source terms attributable to the pressure derivative and $\delta v/\Delta t \Phi^0$, and S_P^ϕ, contains the convecting errors and the time dependent terms. Note that since the convecting error,

$$\sum\left[\frac{(\rho\mathbf{V})\cdot\mathbf{A}}{\bar{\rho}}\right] \tag{7}$$

does not include density in this variable option, Eq. (7) refers to "volume errors" instead of "mass errors". It should be pointed out that in order to balance the second-order artificial viscosity appearing in numerical dissipation model, the retarded density $\bar{\rho}$ (see Eq. 8) should be used here.

2.2 *Numerical Dissipation*

A variety of numerical dissipation models are used to suppress the spurious odd and even point oscillations and to dampen nonphysical overshoots near shock waves. Numerical dissipation models have to fulfill the requirements of determining how much of the dissipation should be included and when or where the different terms should be switched on or off. Most of them use a combination of second-plus-fourth order terms[1-3,20,21], either explicitly or implicitly. All of these second-plus-fourth order models have the common feature that they are expressed in the dependent variable Φ, ($\rho, \rho U, \rho V$ and ρE), used in the concerned Φ-equation. In this work we use an implicit numerical dissipation model which includes the second-plus fourth-order terms expressed in pressure for all transport equations. The fourth-order terms of the numerical dissipation model come from the use of Rhie-Chow interpolation[9], and the second-order terms are due to the use of retarded density expressed as

$$\bar{\rho} = \rho - \mu\Delta\xi\vec{\rho}_\xi = \rho - \mu\Delta\xi c^2\vec{P}_\xi. \tag{8}$$

where c is the sound speed, μ is a smoothing function, $\vec{P}_\xi$ is upwind biased difference with respect to ξ.

To get fourth-order difference of pressure, we first subtract the pressure gradient $(\partial P/\partial \xi_j)$ from the ρU-equation at the cell-center which gives $(\rho U)^{\#}$. Then we interpolate $(\rho U)^{\#}$ to the cell-face, and add the pressure gradient $(\partial P/\partial \xi_j)$. The same strategy is used for ρV-equation. It can be shown that this procedure of subtracting and adding the pressure gradient is equivalent to adding third-order pressure derivative, i.e.

$$(\rho U)_{i+1/2,j} = \tfrac{1}{2}[(\rho U)_{i+1,j} + (\rho U)_{i,j}] - \alpha \nabla^3 P \tag{9}$$

where

$$\alpha = \delta v / 4 \Delta x a_p$$

$$\nabla^3 P = -(P_{i+2,j} - 3P_{i+1,j} + 3P_{i,j} - P_{i-1,j})$$

where a_p is the diagonal coefficient in the discretized Φ-equation (see Eq. 6), and $\nabla^3 P$ is a third-order central differencing term. After this treatment, the convecting velocity at the face can be obtained from the relation

$$U_{i+1/2,j} = \frac{(\rho U)_{i+1/2,j}}{\bar{\rho}_{i+1/2,j}}$$

where $\bar{\rho}$ is retarded density expressed in Eq. (8).

The final artificial dissipation model for uniform grid and two-dimensional flow, for example, can be explicitly written as:

$$DP = D_x P + D_y P \tag{10}$$

where $D_x P$ and $D_y P$ are the contributions for the two coordinate directions, respectively, which have the form (for $U_\eta, U_\xi > 0$):

$$D_x P = \{d_{i+1/2,j} - d_{i-1/2,j}\};$$

$$D_y P = \{d_{i,j+1/2} - d_{i,j-1/2}\}. \tag{11}$$

The d's in the above equation can be written (see Appendix)

$$d_{i+1/2,j} = A_x \mu_{i+1/2}(P_{i+1/2,j} - P_{i-1/2,j}) + B_x(P_{i+2,j} - 3P_{i+1,j} + 3P_{i,j} - P_{i-1,j}) \tag{12}$$

where A and B are coefficients imposed by momentum and state equations. This model with a special smoothing function has been found to satisfy the requirements for both internal and external flows.

The traditional smoothing function in Eq. (8) has the form[7,11,12]

$$\mu^0_{i+1/2} = \max\left\{0., K_0\left[1 - \left(\frac{M_{ref}}{M_{i+1/2}}\right)^2\right]\right\} \tag{13}$$

which is used to enhance the stability at supersonic regions. For this function, we found that M_{ref} has to be chosen smaller than sonic Mach number, otherwise oscillations or

even stability problems occur. On the other hand, too small M_{ref} gives smearing at shocks. Consequently, using the traditional smoothing function either introduces excessive dissipation, ($M_{ref} < 1.$), leading to smearing of the sharp physical discontinuities at shocks, or gives too little dissipation, ($M_{ref} = 1.$), resulting in unphysical oscillations. In order to avoid this problem a second smoothing function has been chosen to suppress the oscillation when M_{ref} is set to close to sonic.

The second-level filter has the form

$$\mu^1_{i+1/2} = \max\left\{0., K_1\left[-\left(\frac{\gamma_{ref}}{\gamma_{i+1/2,j}}\right)^2\right]\right\} \tag{14}$$

where

$$\gamma_{i+1/2,j} = \max(\gamma_{i+1,j}, \gamma_{i,j})$$

and

$$\gamma_{i,j} = \frac{|M_{i+1,j} - 2M_{i,j} + M_{i-1,j}|}{|M_{i+1,j} + 2M_{i,j} + M_{i-1,j}|}$$

At last a two-level filtering smoothing function is designed as

$$\mu_{i+1/2} = \max\{\mu^0_{i+1/2}, \mu^1_{i+1/2}\} \tag{15}$$

where K_0 and K_1 are the first-level and second-level filtering constants. The first-level filter is used to enhance the stability in supersonic region. The second-level filter is used to dampen the nonphysical oscillation at the shock regions. Note that when the second-level filter is switched on the first-level filter will be switched off to make sharp physical discontinuities.

The implicit dissipation model used in the present study is implemented according to Eqs. (8, 9) and (15). Above we have shown that this implicit dissipation model is similar to the model of Jameson[1]. There are two main differences between the present dissipation model and Jameson's model:

i) In Jameson's model, the dissipation terms are explicitly expressed in Φ ($\rho, \rho U, \rho V$ and ρE) when used in the relevant Φ-equation, whereas in the present scheme $d_{i+1/2,j}$ is expressed in P only.

ii) In Jameson's dissipation model, both second and fourth differences need adjusting of the numerical constant and the fourth difference terms have to be switched off at shock waves[22]; in the present scheme only the second difference term needs a numerical constant to ensure proper shock capturing properties.

The numbers for K_0 K_1 M_{ref} and γ_{ref} are 1.0, 0.2–0.5, $\sim$ 1.0 and 0.125 respectively. The numerical investigations have shown that this model gives good discontinuity resolution at shock waves for both internal and external flows.

The details of the present model are given in the Appendix.

2.3 *Pressure Correction Equation*

The advantage of the pressure-based schemes is that they are efficient for both compressible and incompressible flows. Therefore, they are often argued to be an algorithm for all speed flows[7,15].

To obtain the pressure correction.equation, the flux for mass conservation law in Eq. (1) can be divided into one previous time step value $\dot{m}^0$, and one correction $\dot{m}'$ so that

$$\dot{m} = \dot{m}^0 + \dot{m}' \tag{16}$$

The mass flux corrections on the control volume surfaces can be approximated by truncating the momentum equations to get a relationship of mass correction and pressure correction as follows[5,14]

$$(\rho u)'_j = -\frac{\delta v}{a_P}\frac{\partial P'}{\partial x_j}.$$

The mass flux at east face, for example, becomes

$$\dot{m}'_{i+1/2} = (\mathbf{A}\cdot(\rho u)'_j)_{i+1/2} = -\left(\frac{\delta v}{a_P}\mathbf{A}\cdot\nabla P'\right)_{i+1/2}. \tag{17}$$

Substituting Eqs. (16) and (17) into the continuity equation we obtain

$$(\rho_P - \rho_P^0)\frac{\delta v}{\Delta t} + \sum_{m=1}^{4}\left(\frac{\delta v}{a_P}\mathbf{A}\cdot\nabla P'\right) + \Delta\dot{m}_P = 0 \tag{18}$$

where $\Delta\dot{m}_P$ is the continuity error. Note that the term $(\rho_P - \rho_P^0)$ represents the density correction ρ'_P at the center of the control volume during the time step. It is assumed that density correction can be related to pressure correction according to Eq. (2), i.e.

$$\rho' = \frac{\gamma P'}{(\gamma - 1)(H_0 - 0.5|\mathbf{V}|^2)} \tag{19}$$

Of course, this manipulation gives the pressure correction equation a hyperbolic appearance with respect to time. Note that as Mach number becomes small and density gradients become negligible, the quasi-time-dependent term disappears and the scheme degenerates to the standard iterative scheme for incompressible flow. In the curvilinear coordinates, the diffusion term of Eq. (18) forms

$$(\mathbf{A}\cdot\nabla P')_{i+1/2} = \left\{|\mathbf{A}|\mathbf{n}\cdot\mathbf{g}_1 g^{1j}\frac{\partial P'}{\partial \xi_j}\right\}_{i+1/2}$$

which can be rewritten so that

$$\{\mathbf{A}\cdot\nabla P'\}_{i+1/2} = D_{\xi i+1/2}(P'_{i+1} - P'_i) + D_{\eta i+1/2}(P'_{i+1/2,j+1/2} - P'_{i+1/2,j-1/2})$$

where the D's contain the metrics of the grid. The last term which represents non-orthoganal effect is neglected. This is permissible, since the pressure correction equation is a *correction* equation with the sole object of satisfying continuity equation, i.e. achieving $\Delta\dot{m}_P = 0$ (see Eq. 18). The discretized equation for P' can also be cast into the form

$$a_P P'_P = \sum a_{nb} P'_{nb} + S_C \tag{20}$$

where S_C is mass residual.

3. BOUNDARY CONDITIONS

Generally speaking, the boundary conditions for inviscid internal and external flows do not necessarily need to be different. The common treatment is a combination of the given physical boundary conditions and numerical boundary conditions according to the theory of characteristics. At a solid surface, only pressure is required, since the the normal component of velocity is identical to zero. The pressure derivative $\partial P/\partial n$ at the solid surface can be determined from the normal momentum equation[23]. Then the pressure at the wall can be estimated by extrapolation from the pressure at the adjacent values, using the known $\partial P/\partial n$.

In our experience, a first-order extrapolation, e.g., assuming the second derivative in the normal direction to be zero, for both pressure and tangential component of velocity, is sufficiently accurate for the present test cases. The density at the wall then can be extracted by enforcing constant free stream enthalpy at the wall[3].

It is generally required that the far-field boundary (or outlet boundary for internal flow) should be far enough, so that the far-field flow can be considered to be undisturbed, or where some known properties can be specified along the boundaries, such as pressure at outlet in internal flows. This region is in fact very large for external flows. Some numerical experiments[3] show that the far-field boundary should be set 98 or more chord length away from the airfoil, to ensure adequate accuracy for airfoil flows.

In this paper, a non-reflecting[24] far-field boundary condition is used for the airfoil flow. The boundary conditions are based on the theory of characteristics for locally one-dimensional inviscid flow. For supersonic inflow or outflow, the local one-dimensional Riemann invariants, entropy and tangential velocity component,

$$R_1 = \mathbf{V}\cdot\mathbf{n} - \frac{2}{\gamma-1}c, \quad R_2 = \mathbf{V}\cdot\mathbf{n} + \frac{2}{\gamma-1}c$$

$$R_3 = \ln\left(\frac{P}{\rho^\gamma}\right), \quad R_4 = \mathbf{V} - (\mathbf{V}\cdot\mathbf{n})\mathbf{n}$$

are given from outside or inside the computational region, respectively. For subsonic inflow, R_1, R_3, and R_4 are given from outside and R_2 from inside, while for subsonic outflow, R_2, R_3, and R_4 are determined from inside and R_1 from outside. These four quantities provide a complete definition of the flow at the far-field boundary.

Since the computation domain is a finite region, the blockage effect of the airfoil influences the *free stream* velocity at the far-field boundaries. This can be taken into account by using the far-field circulation correction to modify free stream velocity[1-3,23]. According to the compressible potential vortex solution, the compressible potential, with reference to a polar coordinate system centered at the hydrodynamic center of the airfoil, reads

$$\phi = |\mathbf{V}_\infty| r\cos(\theta - \alpha) + \frac{\Gamma}{2\pi}\tan^{-1}(\beta\tan(\theta - \alpha)) + \ldots$$

where the circulation $\Gamma = 1/2 M_\infty B C_L$, B is the chord length, C_L the coefficient of lift at the surface, α the angle of attack, $\beta = \sqrt{1 - M_\infty^2}$ and r, θ are polar coordinates with origin at the hydrodynamic center, which is located at the quarter chord point on the NACA0012.

The perturbed free stream velocity can then be obtained as

$$U_\infty = |\mathbf{V}|\cos(\alpha) + \frac{\Gamma}{2\pi r}\frac{\beta\sin(\theta)}{1 - M_\infty^2\sin^2(\theta - \alpha)}$$

$$V_\infty = |\mathbf{V}|\sin(\alpha) + \frac{\Gamma}{2\pi r}\frac{\beta\cos(\theta)}{1 - M_\infty^2\sin^2(\theta - \alpha)}$$

For the internal test case presented, to get better convergence, the traditional boundary conditions are used. At the inlet, the total temperature and velocity are specified with the extrapolation of the pressure. The pressure is specified at outlet, and the remaining variables are extrapolated.

The boundary conditions for the pressure correction P', either at the wall or at far-field boundaries, are obtained using first-order extrapolation.

4 RESULTS AND DISCUSSION

To validate the proposed scheme, two test cases are presented, one internal flow and one external flow with various free stream conditions.

4.1 Internal Flow Simulation

For bounded transonic flow, we present the computational results for a quasi-one-dimensional flow in a converging-diverging nozzle which is an excellent and revealing test case. Other computation results for internal flows have been reported in Ref. 29.

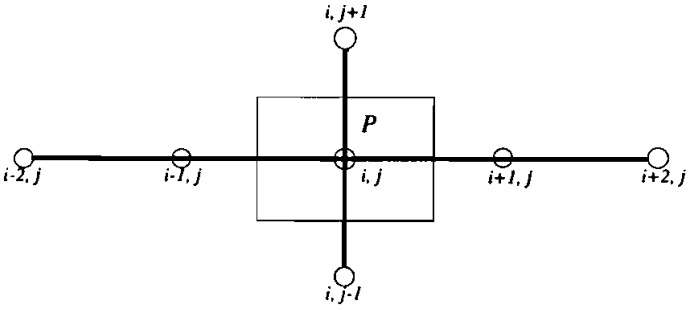

Figure 1 The control volume.

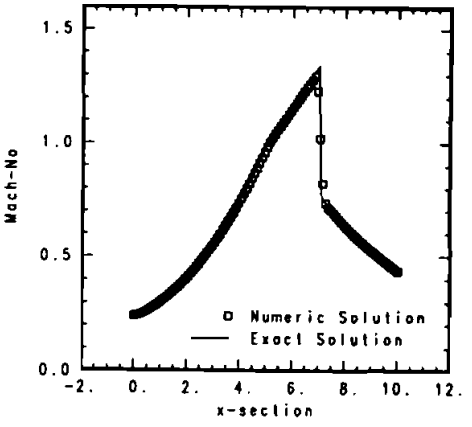

Figure 2 Mach number from 2D-solution.

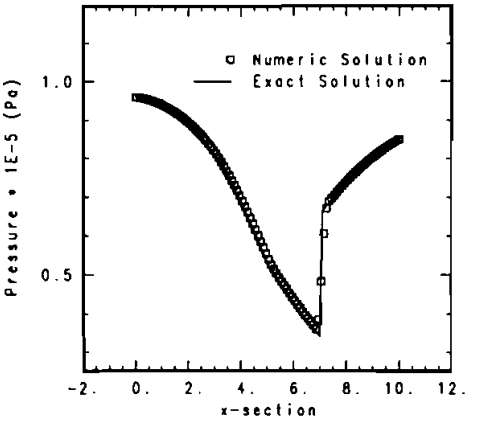

Figure 3 Pressure distributions from 2D-solution.

The cross-section area[26] S of the chosen nozzle is given by:

$$S = 1 + \frac{3}{2}\left(1 - \frac{x}{5}\right)^2, \quad 0 \le x \le 5$$

$$S = 1 + \frac{1}{2}\left(1 - \frac{x}{5}\right)^2, \quad 5 \le x \le 10.$$

Unlike most papers which have presented quasi-one-dimensional results, we compute this flow in two-dimensional fashion with the grid distribution 100×5 for a piece of prism, because of axial symmetry, which has the varying cross-section area according to the above formula. The Mach number and pressure distribution at the center line of the nozzle are presented in Figures 2 and 3.

The initial conditions for U, P and T were obtained by linear interpolation between the exact inflow and outflow values. At the inlet, the total temperature $T_0 = 300$ K, and the Mach number $M_0 = 0.241$. The static pressure is specified to be $P_{\text{outlet}} = 0.85 \times 10^5$ at the outlet. All other properties are extrapolated from the internal field. The continuity error scaled by total incoming mass flux is used as convergence criterion, which is 10^{-5}. The first-order upwind scheme is used for this computation. The agreement between calculations and the analytical solution is excellent.

4.2 *External Flow Simulation*

An unbounded flow over airfoil NACA0012 is chosen to demonstrate external flow simulation. The inviscid flow cases around this airfoil have been extensively studied using many density-based methods. Unfortunately no calculations using the pressure-based method have been reported in the literature.

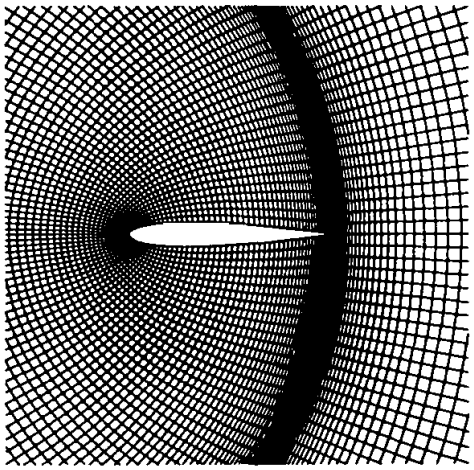

Figure 4 C-grid 196 × 62, Enlargement in vicinity of surface.

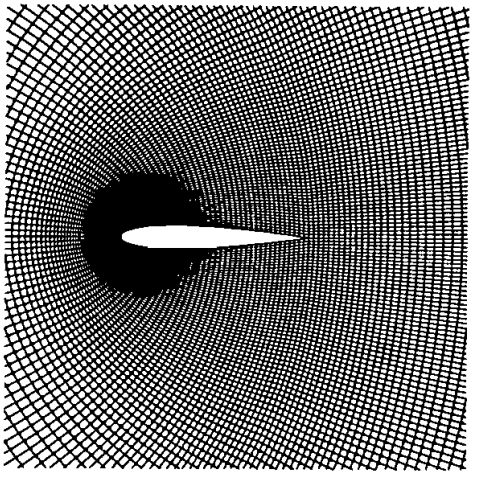

Figure 5 C-grid 250 × 78, Enlargement in vicinity of surface.

The two-dimensional parabolic C-meshes[26] which are used in this study are shown in Figures 4 and 5. The far-field boundaries of mesh are located approximately ~ 6 chords from the airfoil for the mesh of 250 × 78 cells and 3.5 chords for the mesh of 196 × 32 cells. 100 cells for the mesh of 250 × 78 and 120 nodes for the mesh of 196 × 32 are located at the surface of the airfoil. The calculations are initialized with a uniform free stream flow at the prescribed Mach number and angle of attack. The convergence criterion is given as

$$|R|_2 = \left\{ \frac{1}{N} \sum_{i,j} (R_{i,j})^2 \right\}^{1/2}$$

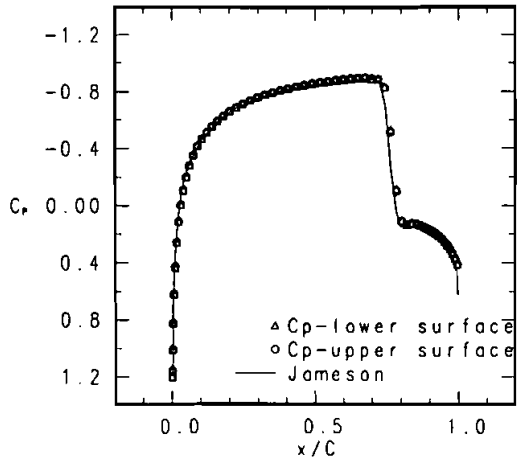

Figure 6 Surface pressure distribution, $M_\infty = 0.85$, $\alpha = 0.0$.

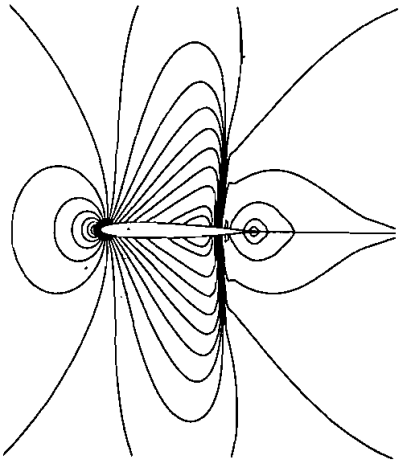

Figure 7 Pressure contours, $M_\infty = 0.85$, $\alpha = 0.0$.

where $R_{i,j}$ is the residual of continuity equation $|\Delta\rho/\Delta t|$ for cell (i,j) and N is the total number of control volumes. For a converged solution, the residual is reduced by 5 decades.

The predicted pressure coefficients and pressure contours are presented in Figure 6 and Figure 7 for free-stream Mach number $M_\infty = 0.85$ and angle of attack $\alpha = 0°$. The 196×32 mesh is used. The present results are compared with those of Jameson and Yoon[2]. The results are almost identical, as may be seen in the figure.

Figure 8 presents the surface pressure distribution, compared with those of Caughey[27], for the airfoil at a free-stream Mach number of 0.80 and 1.25° angle of attack with the mesh 250×78 cells. Figure 9 shows the pressure contours. Again the

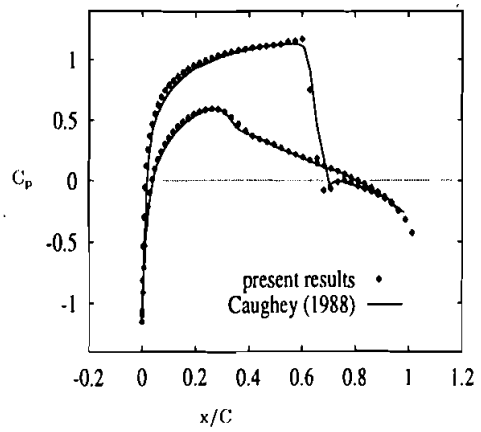

Figure 8 Surface pressure distribution, $M_\infty = 0.8$, $\alpha = 1.25$.

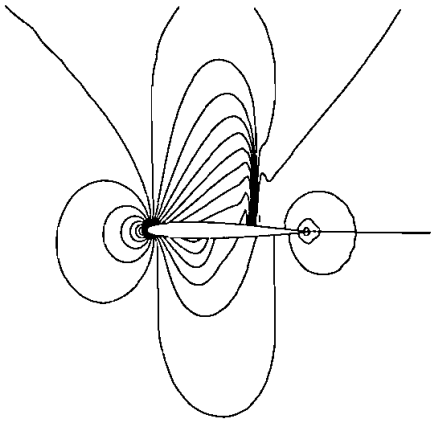

Figure 9 Pressure contours, $M_\infty = 0.8$, $\alpha = 1.25$.

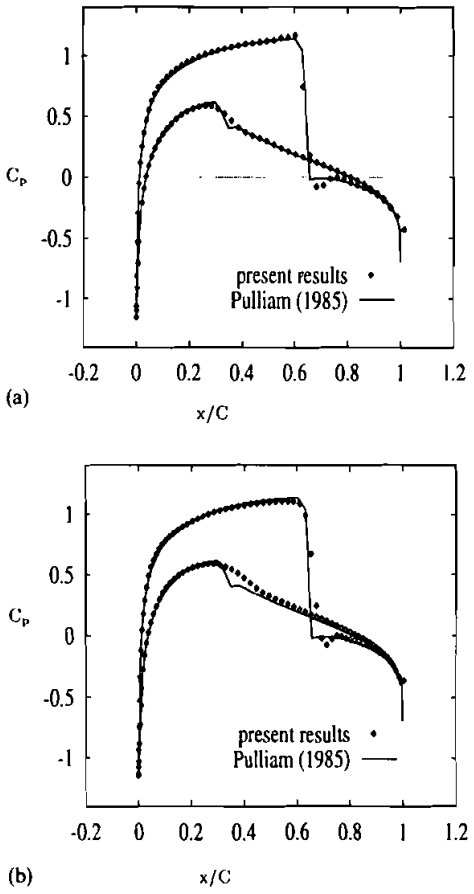

Figure 10 Comparison between new (above) and old (below) smoothing functions, $M_\infty = 0.8$, $\alpha = 1.25$.

agreement between the results obtained from the presented pressure-based method and those from Ref. 27 which is the time-marching method is very good.

The comparison between new and old smoothing functions are shown in Figure 10. The benefits of using two-level filtering smoothing function are obvious. Since the traditional function introduces excessive dissipation due to use of a smaller M_{ref}, smearing appears at the weak shock on the lower surface of the airfoil.

For $M_\infty = 0.85$, $\alpha = 1°$, the coefficient of pressure in Figure 11 and the pressure contours in Figure 12 are shown. The results are also compared with those of Ref. 3. The agreement is good for global parameters and shock locations. The difference at shocks is primarily a result of the finer grid density (560 × 65) and grid clustering used in the Pulliam calculation. It is interesting to note that although high lever clustering of

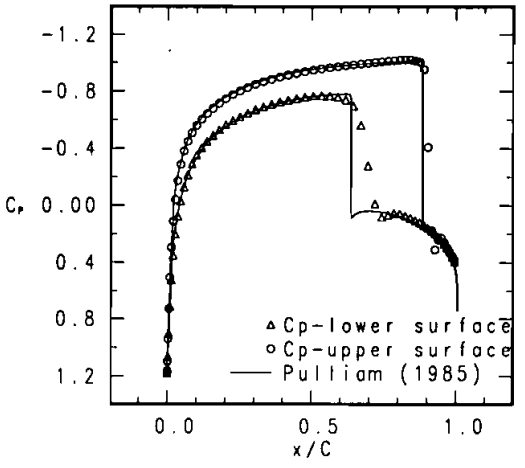

Figure 11 Surface Pressure distribution, $M_\infty = 0.85$, $\alpha = 1.00$.

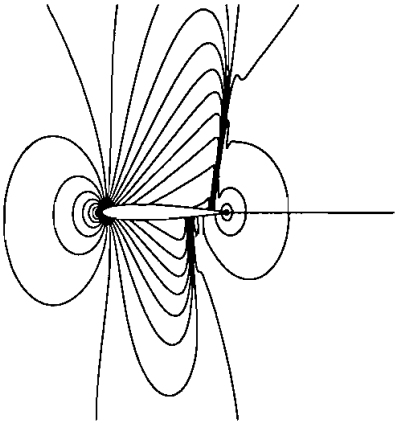

Figure 12 Pressure contours, $M_\infty = 0.85$, $\alpha = 1.00$.

Table 1 The global parameters

Author	grid type	grid distribution	B. C. Distance × chord	C_L	C_D	C_M
		Global Parameter of NACA0012, $M_\infty = 0.85$, $\alpha = 0.00°$				
Jameson[1]	O	128 × 32	—	0.0	0.0471	0.0
Present	C	250 × 78	6/6/6	0.0	0.0559	0.0
		Global Parameter of NACA0012, $M_\infty = 0.8$, $\alpha = 1.25°$				
Jameson[1]	O	128 × 32	—	0.3513	0.0230	−0.0377
Caughey[28]	C	192 × 32	50/100/50	0.3695	0.0237	−0.0432
Pulliam[3]	C	235 × 33	24/48/48	0.3618	0.0236	−0.0411
Present	C	250 × 78	6/6/6	0.3575	0.0220	−0.0375
		Global Parameter of NACA0012, $M_\infty = 0.85$, $\alpha = 1.00°$				
Pulliam[3]	C	569 × 65	24/48/48	0.3938	0.0604	−0.1393
Present	C	196 × 32	3/3.5/3	0.3890	0.0662	−0.1282

the grid is used in Ref. 3, the shock is still smeared out over 3–4 cells, similar to the present calculations where a rather coarse mesh (196 × 32) is used.

It was found that there are not significant differences in predicted results between the use of the first-order upwinding scheme and second-order MUSCL scheme. Hence all the results presented in this paper are obtained by using the first-order upwinding scheme. The present global parameters are compared with the predictions of Jameson, Caughey and Pulliam in Table 1. From Table 1, we can see that the agreement between these predictions is quite good. All the lift and moment coefficients obtained from different authors are in the same order. However, the present drag coefficients for $M_\infty = 0.85$, $\alpha = 0.0°$ and $M_\infty = 0.85$, $\alpha = 1.0$ are larger than others. This is due to the lower pressure recovery at the trailing edge. We believe that the coarse mesh in j-direction (See Figure 4) close to the trailing edge leads to lower pressure resolution in this high gradient region. This lower resolution also appeared in Ref. 28.

5. SUMMARY

A pressure-based Euler procedure has been developed and applied to both internal and external transonic flows. A numerical dissipation model adopted in the present procedure is described. A smoothing function, which includes a two-level filter, is used to adjust the second dissipation. The results demonstrate that the pressure-based method with the present numerical dissipation model, is capable of successful simulation of both internal and external transonic flows. No special method for convergence acceleration has been introduced. We believe that the multigrid method[5,8,18,28] will be very useful in improving the convergence rates.

Acknowledgments

The authors wish to thank Prof. Per Lötstedt, Saab Military Aircraft, for providing the grid generator.

References

1. Jameson, A., Schmidt, W. and Turkel, E. (1981) "Numerical Solutions of the Euler Equations by Finite Volume Methods Using Runge-Kutta Time-Stepping Schemes," AIAA paper 81-1259.
2. Rizzi, A., (1984) "Spurious Entropy and Very Accurate Solutions to the Euler Equations", AIAA Paper 84-1644.
3. Pulliam, T. H. and Barton, J. T., (1985) "Euler Computations of AGARD Working Group 07 Airfoil Test Cases", AIAA paper 85-0018.
4. Chorin, A. J., (1967) "A Numerical Method for Solving Incompressible Viscous Flow Problems," *Journal of Computational Physics*, **2**, 12–26.
5. Patankar, S. V., (1980) "*Numerical Heat Transfer and Fluid Flow*", McGraw-Hill, Washington.
6. Issa, R. I., (1986) "Solution of the Implicitly Discretized Fluid Flow Equations by Operator-Splitting." *Journal of Computational Physics*, **62**, 40–65.
7. Karki, K. C. and Patankar, S. V. (1989) "Pressure based Calculation Procedure for Viscous Flows at All Speeds in Arbitrary Configurations," *AIAA Journal*, **27**(9), 1167–1174.
8. Zhou, G. and Davidson, L., (1992) "Transonic Flow Computation Using a Modified SIMPLE Code Based on Collocated Grid Arrangement", *Proc. First European CFD Conference*, Brussels, **2**, 749–756.
9. Rhie, C. M., (1986) "A Pressure Based Navier-Stokes Solver Using the Multigrid Method", AIAA paper 86-0207, Reno, January.
10. Rhie, C. M. and Chow, W. L., (1984) "Numerical Study of the Turbulent Flow Past an Airfoil with Trailing Edge Separation", *AIAA Journal*, **21**, 1527–1532.
11. McGuirk, J. J. and Page, G. J., (1990) "Shock Capturing Using a Pressure-Correction Method", *AIAA Journal*, **28**(10), 1751–1757.
12. Lien, F. S. and Leschziner, M. A., (1993) "A Pressure-Velocity Solution Strategy for Compressible Flow and Application to Shock/Moment Turbulence Closure", *ASME Journal Fluid Engineering*, **115**, 717–725.
13. Wornom, S. F. and Hafez, M., (1986) "Calculation of Quasi-One-Dimensional Flows with Shocks", *Computers and Fluids*, **14**(2), 131–140.
14. Davidson, L. and Farhanieh, B., (1992) "A Finite-Volume Code Employing Collocated Variable Arrangement and Cartesian Velocity Components for Computation of Fluid Flow and Heat Transfer in Complex Three-Dimensional Geometries", Rept. 92/4, Thermo and Fluid Dynamics, Chalmers University of Technology, Gothenburg.
15. Shyy, W. and Chen, M. H., (1992) "Pressure-Based Multigrid Algorithm for Flow at All Speeds", *AIAA Journal*, **30**(11), 2660–2669.
16. van Leer, B., (1979) "Towards the Ultimate Conservation Difference Scheme V: A Second-order Sequel to Godunov's Method", *Journal of Computational Physics*, **32**, 101–132.
17. Leonard, B. P., (1979) "A Stable and Accurate Convective Modelling Procedure Based on Quadratic Up-stream Interpolation", *Computer Methods in Applied Mechanics and Engineering*, **19**, 59–97.
18. Zhou, G., Davidson,. L. and Olsson. E., (1994) "Transonic Inviscid/ Turbulent Airfoil Flow Simulations Using a Pressure Based Method with High Order Schemes", *14th International Conference on Numerical Method in Flow Dynamics*, 11–15 July 1994, Bangalore, India.
19. Anderson, J. D., (1990) *Modern Compressible Flow*, McGraw-Hill Publishing Company, New York.
20. Chen, Y. S. (1988) "Viscous Flow Computations Using a Second-Order Upwind Differencing Scheme", AIAA paper, 88-0417, January.
21. Swanson, R. C. and Turkel, E., (1987) "Artificial Dissipation and Central Difference Schemes for the Euler and Navier-Stokes Equations", AIAA paper 87-1107, June.
22. Schmidt, W. and Jameson, A., (1985) "Euler Solvers as an Analysis Tool for Aircraft Aero-dynamics", *Advances in Computational Transonics*, edited by *Habashi, W. G., Swansea*, Pineridge Press, pp. 371–403.
23. Rizzi, A., (1978) "Numerical Implementation of Solid Body Boundary Conditions for the Euler Equation", Zeitschrift Für Angewandte Mathematik und Mechanik, **24**(7), 301–304.
24. Rizzi, A. and Müller, B., (1989) "Large-Scale Viscous Simulation of Laminar Vortex Flow Over a Delta Wing," *AIAA Journal*, **27**(7), 833–840.
25. Casier, F., Deconinck, H. and Hirsch, Ch., (1984) "A Class of Bidiagonal Schemes for Solving the Euler Equations", *AIAA Journal*, **22**(11), 1556–1563.
26. Lötstedt, P., (1993) "Privat communication". Saab Military Aircraft, Linköping, Sweden
27. Caughey, D. A., (1988) "Diagonal Implicit Multigrid Algorithm for the Euler Equations", *AIAA Journal*, **26**(7), 841–851.
28. Johansson, P. and Davidson, L., (1994) "A Full Multigrid Method Applied to Tufbulent Flow Using the SIMPLEC Algorithm Together with a Collocated Grid Arrangement", Multigrid method IV, selected paper, pp. 245–256, Birkhäuser Verlag.

29. Zhou, G., Davidson, L. and Olsson, E., (1994) "Shock Capturing Using An Improved Pressure Based Method with Semi-Retarded Density Concepts", Rept. 1994, Thermo and Fluid Dynamics, Chalmers University of Technology. Gothenburg.

APPENDIX

In this appendix we show that the present scheme, which *implicitly* introduces numerical dissipation through Rhie-Chow interpolation and retarded density, is equivalent to an *explicit* second- and fourth-order numerical dissipation model expressed in pressure.

The proposed model can be deduced using an 1-*D* model problem in Cartesian frame represented as

$$\frac{\partial \Phi}{\partial t} + \frac{\partial}{\partial x}(U\Phi) = -\frac{\partial P}{\partial x} \tag{21}$$

where $\Phi = \rho U$. The integrated form of Eq. (21) is

$$(AU\Phi)_{i+1/2} - (AU\Phi)_{i-1/2} = -\frac{\partial P}{\partial x}\delta v - \frac{\partial \Phi}{\partial t}\delta v \tag{22}$$

For the convecting velocity U, using Rhie-Chow interpolation for mass flux, we have

$$U_{i+1/2} = \frac{1}{\rho_{i+1/2}}(F_x\Phi_{i+1} + (1-F_x)\Phi_i - \alpha\nabla^3 P) = \frac{1}{\rho_{i+1/2}}(\Phi^c_{i+1/2} - \alpha\nabla^3 P) \tag{23}$$

where superscript c denotes that Φ^c is computed using central differencing. F_x is the interpolation factor. Substituting Eq. (23) into Eq. (22) we get:

$$\left[A\left(\frac{\Phi^c}{\rho}\right)\Phi\right]_{i+1/2} - \left[A\left(\frac{\Phi^c}{\rho}\right)\Phi\right]_{i-1/2} - \left[\frac{A_{i+1/2}}{\rho_{i+1/2}}\right]\alpha\nabla^3 P\Phi_{i+1/2} + \left[\frac{A_{i-1/2}}{\rho_{i-1/2}}\right]\alpha\nabla^3 P\Phi_{i-1/2}$$

$$= -\frac{\partial P}{\partial x}\delta v - \frac{\partial \Phi}{\partial t}\delta v \tag{24}$$

In order to introduce the second-order dissipation, the retarded density concept ($\vec{\rho} = \rho - \mu\Delta x\vec{\rho}_x$) is used to replace the real density in equation (24) in term Φ^c/ρ. We get

$$\left(\frac{\Phi^c}{\vec{\rho}}\right)_{i+1/2} \simeq \left(\frac{\Phi^c}{\rho}\right)_{i+1/2}\left(1 + \frac{\mu_{i+1/2}}{\rho_{i+1/2}}\Delta x\vec{\rho}_x\right); \quad \left(\frac{\Phi^c}{\vec{\rho}}\right)_{i-1/2} \simeq \left(\frac{\Phi^c}{\rho}\right)_{i-1/2}\left(1 + \frac{\mu_{i-1/2}}{\rho_{i-1/2}}\Delta x\vec{\rho}_x\right)$$

where $\vec{\rho}_x$ is upwind biased difference with respect to x. Note that with the help of the relation $P_x \simeq c^2\rho_x$ and $P = (c^2/\gamma)\rho$, (where c is sound speed), the retarded density

concept here is the same as the *real pressure* concept ($P_i = \bar{P}_i - \mu_{i-1/2}(\bar{P}_i - \bar{P}_{i-1})$), proposed in Ref. (11), which is used to extract the density.

Replacing Φ^c/ρ by $\Phi^c/\bar{\rho}$ in Eq. (24) using the above formula, we obtain

$$\left[A\left(\frac{\Phi^c}{\rho}\right)\Phi\right]_{i+1/2} - \left[A\left(\frac{\Phi^c}{\rho}\right)\Phi\right]_{i-1/2} + A_{i+1/2}\left[\frac{\mu_{i+1/2}}{\rho_{i+1/2}}\right]\left[\frac{\Phi_{i+1/2}}{\rho_{i+1/2}}\right]\Phi_{i+1/2}\Delta x\vec{\rho}_x$$
$$- A_{i-1/2}\left[\frac{\mu_{i-1/2}}{\rho_{i-1/2}}\right]\left[\frac{\Phi_{i-1/2}}{\rho_{i-1/2}}\right]\Phi_{i-1/2}\Delta x\vec{\rho}_x - \alpha\left[\frac{A_{i-1/2}}{\rho_{i-1/2}}\right]\nabla^3 P\Phi_{i-1/2}$$
$$+\alpha\left[\frac{A_{i-1/2}}{\rho_{i-1/2}}\right]\nabla^3 P\Phi_{i-1/2} + HOT = -\frac{\partial P}{\partial x}\delta v - \frac{\partial \Phi}{\partial t}\delta v \tag{25}$$

where HOT represents the higher order terms, which are the product of the second-order and fourth-order terms. With the help of the relation $P_x \simeq \rho_x c^2$, and rearranging the equation as Eq. (25), using the notation

$$\frac{\Phi^c}{\rho} = U^c$$

we get an artificial dissipation model for 1-D problem as follows:

$$(AU^c\Phi)_{i+1/2} - (AU^c\Phi)_{i-1/2} + D_x P = -\frac{\partial P}{\partial x}\delta v - \frac{\partial \Phi}{\partial t}\delta v. \tag{26}$$

Here $D_x P$ have the same form as in Eq. (10), i.e.

$$D_x P = \{d_{i+1/2,j} - d_{i-1/2,j}\}.$$

Each term in the above equation has a similar form

$$d_{i+1/2,j} = A_x\mu_{i+1/2}(P_{i+1/2,j} - P_{i-1/2,j}) + B_x(P_{i+2,j} - 3P_{i+1,j} + 3P_{i,j} - P_{i-1,j}) \tag{27}$$

where the coefficients A and B are given as follows:

$$A_x = \left[\left(\frac{A}{c^2}\right)\left(\frac{\Phi^2}{\rho^2}\right)\right]_{i+1/2}$$

and

$$B_x = \frac{1}{4}\left[\left(\frac{A\delta v}{\Delta x a_P}\right)\left(\frac{\Phi}{\rho}\right)\right]_{i+1/2}.$$